Tip Leakage Vortex Cavitation from the Tip Clearance of a Single Hydrofoil

Seiji HIGASHI, Yoshiki YOSHIDA*, and Yoshinobu TSUJIMOTO

Osaka University, Graduate School of Engineering Science
1-3, Machikaneyama, Toyonaka, Osaka 560-8531, Japan
*E-mail: yoshida@me.es.osaka-u.ac.jp

Abstract

Focusing on the tip leakage vortex cavitation, experimental and numerical studies were carried out as the first step of the investigation of cavitations in tip leakage flow. For a single hydrofoil with a tip clearance, tip leakage vortex cavitations were observed for various cavitation numbers and angles of attack. To simulate the tip leakage vortex cavitation, a simple calculation of 2-D unsteady flow based on the slender body approximation with taking into account the effects of cavity growth (Watanabe et al., 2001) was made. The results of calculations show qualitative agreement with the experimental results with respect to the location and size of the cavity. The influences of the cavitation number, angle of attack, blade loading, and the size of tip clearance were simulated reasonably well.

1 Introduction

It is now widely recognized that cavitation instabilities, such as cavitation surge and rotating cavitation, are caused by the unsteady characteristics of cavitation; i.e., mass flow gain factor and cavitation compliance. Cavitations in unshrouded impellers are classified into two types, cavitation on blade surface and cavitation in tip leakage flow. For the blade cavitation, unsteady characteristics have been extensively studied, and it is now possible to predict the mass flow gain factor and cavitation compliance theoretically (Brennen, 1978, and Otsuka et al., 1996). However, few studies have been performed for the cavitation in the tip leakage flow, not only on unsteady characteristics but also on steady behavior. We observe two types of cavitation in the tip leakage flow in experiments. One occurs at the core of the rolled up vortex, and the other occurs at the shear layer between the tip leakage jet and the main flow. The former is called “tip leakage vortex cavitation.” In the present study, we focus on this tip leakage vortex cavitation.

Rains (1954) first proposed to apply the slender body approximation to the tip leakage vortex. In this method, a 3-D tip leakage flow is simulated by a 2-D unsteady crossflow. Chen et al. (1991) applied this method to a compressor tip clearance flow by using the vortex method. In addition, Watanabe et al. (2001) recently extended this method to include the effects of cavity growth, and examined the results by comparing with 2-D unsteady experiments. In the present study, tip leakage vortex cavitations of a single hydrofoil with tip clearance were observed experimentally as 3-D steady flow. The cavitation behavior, the location and size of the cavity, were measured from high-speed video pictures. In addition, Watanabe et al.’s method was applied to predict the tip leakage vortex cavitation. Discussions on the influences of the cavitation number, angle of attack, blade loading distribution, and the size of tip clearance are made to validate this calculation method through the comparison with the experimental results.

2 Nomenclature

C = chord (= 90mm)
C_L = lift coefficient = $\mathrm{Lift}/(\rho U^2 C/2)$
C_p = pressure coefficient = $(p - p_1)/(\rho U^2/2)$
ΔC_p = coefficient of pressure difference on blade surface = $(p_p - p_s)/(\rho U^2/2)$
H = span (= 67mm or 69.2mm)
L = cavity length of blade cavitation
P = pressure
p_1 = pressure at inlet
p_p = pressure on the pressure surface of blade
p_s = pressure on the suction surface of blade
p_v = vapor pressure
p_∞ = reference pressure in unsteady version of Bernoulli equation
Δp = pressure difference across the tip clearance = $p_p - p_s$
q_j = strength of source representing the leakage jet

q_b = strength of source representing the cavity growth
R = radius of cavity
S = distance along the chord
ΔS = increment of S
t = time
Δt = time increment
X, Y, Z = coordinates, defined in Fig. 5
U = velocity of main flow
U_j = velocity of leakage jet flow
α = angle of attack
β = see in Fig. 2 (b)
Γ = strength of vortices
γ = camber (= 1/2 · tanβ)
ν = kinematic viscosity
ρ = density
σ = cavitation number = $(p_1 - p_v)/(\rho U^2/2)$
τ = tip clearance (= 3mm or 0.8mm)

3 Experimental apparatus and procedure

The experiments were conducted by using the cavitation tunnel as shown in Fig. 1. The cross section of test tunnel is square, height and width are 70 mm and 100 mm, and length is 500 mm. A nozzle with area reduction ratio 4.65 is set upstream of the test section.

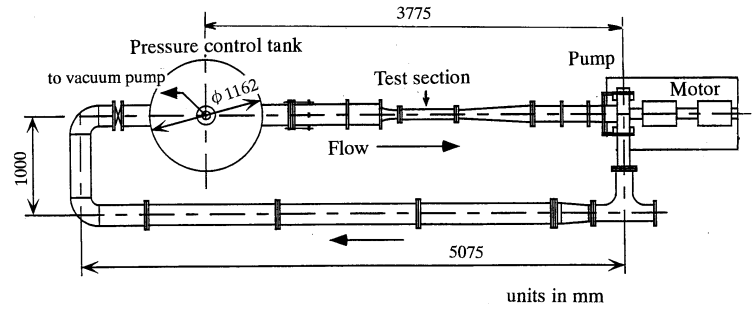

(a) Cavitation tunnel

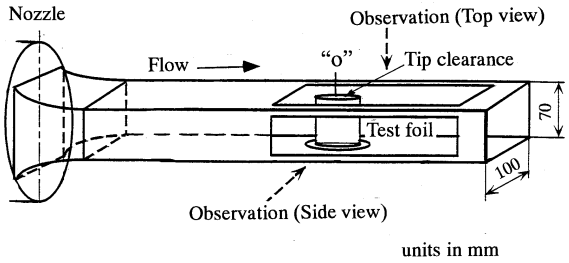

(b) Test section

Figure 1 Cavitation tunnel, and test section

In the present experiment, we used two foils; a flat plate foil, and a circular arc foil. The latter was used to investigate the effect of the distribution of bade loading. Figure 1 shows the configurations of the test foils. The chord C of the foil is 90mm, the span H is 67 mm (for tip clearance 3 mm) or 69.2 mm (for tip clearance 0.8 mm). The camber of the circular arc foil is $\gamma = 1/2 \cdot \tan\beta$ with $\beta = 4$ degrees. The thickness of the foils is constant and 3 mm. Both the leading and trailing edges were rounded with radius R=1.5 mm. With a square tip, "gap cavitation" (Gearhart, 1966) in the clearance between the tip and upper wall, and "sheet vortex cavitation" in the shear layer of the leakage jet is observed. To remove these types of cavitation, the pressure side corner of the tip was rounded with radius R=3 mm, as shown in Fig. 2 (Ido et al., 1991, and Labore et al., 1997).

The angle of attack α can be changed by rotating the foil around the center "O", as shown in Fig. 2. The angles of attack $\alpha = 2,\ 4,\ 6$ degrees for the flat plate foil, and $\alpha = 0$ degree for the circular arc hydrofoil were examined. The

case with the tip clearances τ=3mm (the real value is 2.95 mm), and τ=0.8mm (the real value is 0.83 mm) for the flat plate foil were examined.

Figure 3 shows the lift coefficient, C_L, and the pressure coefficient, C_p, on the foil obtained under the assumption of non-cavitating 2-D incompressible inviscid flow around the thin foil. Although the lift coefficient of the flat plate foil for α=4 degrees is equal to that of the circular arc foil for α=0 degree, the distributions of the pressure difference ΔC_p between the pressure and suction side are different, in particular, near the leading edge.

The velocity of main flow was maintained constant U=5 m/s through the present experiments. Although the effects of Reynolds number were examined within U=4～7 m/s (Re=UC/ν=2.9~5.7×10^5), the influence of Reynolds number on the test results could not be identified in this range. Tap water was used. The water was deaerated by keeping at the lowest pressure (12kPa) for more than 12 hours before the tests.

Both side and top walls of test section were made of transparent acrylic resin, so that we can make visual observations. Two types of observation were made. One is with a high-speed video picture (250 frames/sec records), and the other is with a still camera with strobo light (20μsec). The flow in the vortex core is highly unsteady (Green, 1991, and Arndt et al., 1992), so a single picture is not sufficient to measure the location and size of the tip leakage vortex cavitation. Therefore, the location and size of the cavity were measured by averaging the measurements of many frames of the high-speed video pictures.

We applied the oil film method on the upper wall to visualize the interaction of the leakage flow and the main flow. In addition, we observed the streak of small air bubbles injected at the leading edge to investigate the tip leakage flow in non-cavitating flow.

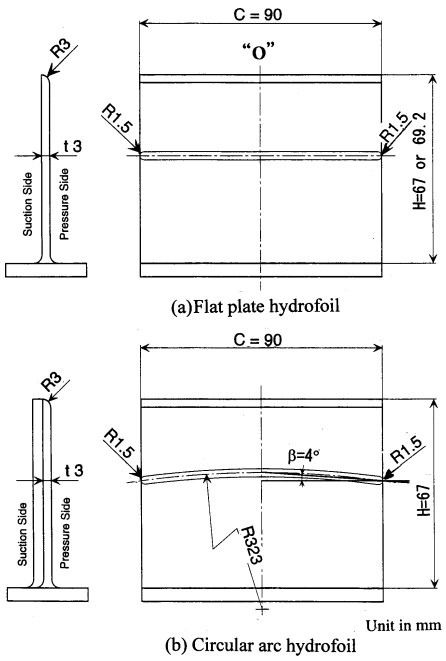

Figure 2 Test hydrofoils

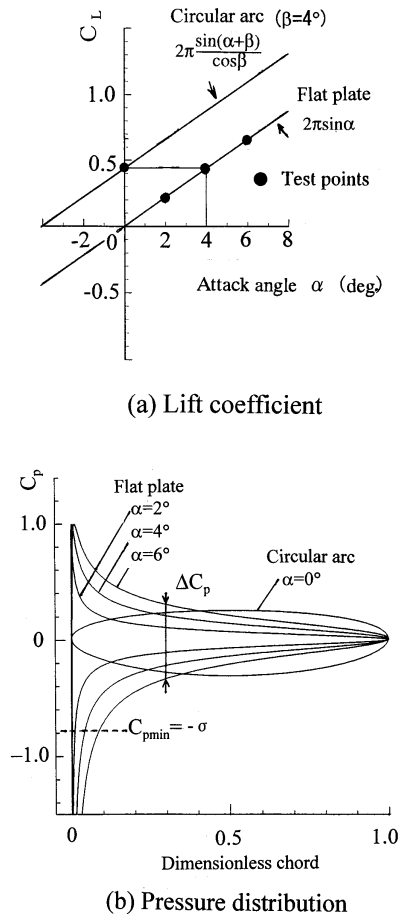

Figure 3 Lift coefficient, C_L, and pressure coefficient, C_p, on the assumption of a thin foil in 2-D potential flow

4 Outline of the analytical method

It is plausible that the tip leakage vortex cavitation occurs in the low pressure region in the vortex core formed by rolling up of the shear layer between the tip leakage flow and the main flow. To explain the calculation method, we illustrate crossflow planes **A**, **B**, **C**, and **D** at different chordwise locations **a**, **b**, **c**, and **d**, respectively, as shown in Fig. 4. Location **a** is at the leading edge and **d** is at the trailing edge. The tip leakage flow starts at location **a**. As the crossflow plane moves through the foil, the vortices representing the shear layer shed into the main flow. The vortices roll up in the subsequent cross sections, as illustrated in planes, **B**, **C**, and **D**. The tip leakage vortex cavitation is expected to occur in the low pressure region in the rolled up vortex core.

We assume that the crossflow plane moves through the foil with the velocity U of the main flow. Hence, the distance between the planes analyzed is $\Delta S=U\times\Delta t$, where Δt is a time increment. The following assumptions were made in the present calculation. The velocity of tip leakage jet on the crossflow plane at location S is simply assumed $U_j = (2\Delta p/\rho)^{1/2}$, where Δp is the pressure difference across the tip clearance estimated from a non-cavitating 2-D incompressible inviscid flow calculation around the thin foil. However, the estimated pressure is lower than the vapor pressure, it is assumed that the pressure there is equal to the vapor pressure.

A vortex method was used for the calculation on the crossflow plane. A source $q_j = 2\times U_j$ is distributed at the tip clearance, which represents the tip leakage jet. The discrete free vortices Γ representing the shear layer between the tip leakage jet and the main flow are released from the corner of the tip. The strength of the vortices is determined as $\Gamma=U_j^2\times\Delta t/2$ from the leakage velocity U_j.

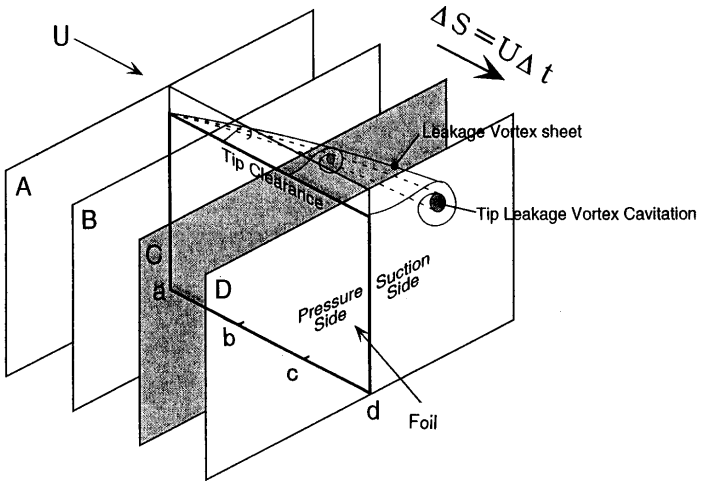

Figure 4 Correspondence of 3-D steady flow with tip leakage vortex cavitation to 2-D unsteady crossflow on plane A~D

It is assumed that a shingle cylindrical cavity starts to develop at the location of the minimum pressure, where the pressure becomes lower than the vapor pressure p_v first. The growth of this cylindrical cavity, radius R, on the crossflow plane is determined by the unsteady version of Bernoulli equation. The reference pressure p_∞ in unsteady version of Bernoulli equation is assumed to be the pressure p_s on the suction surface at the mid-span. The pressure p_s is estimated from a 2-D steady potential flow around the foil. The strength of source $q_b=2\pi R\times dR/dt$ represents the effect of the cavity growth on the flow field, although the size of cavity itself is ignored. The strength q_b is convected on the velocity induced by the source q_j representing the leakage jet, and free vortices Γ representing the shear layer.

The effects of the side walls of the test section are ignored for simplicity. Boundary conditions on the upper wall and the foil are satisfied by introducing the mirror image of singularities within $0\le S/C\le 1.0$ with respect to the upper wall and the foil surface. However, the mirror image with respect to the foil is not considered at $S/C>1.0$ where there

is no foil surface. The initial radius of the cavity is set to be R/C=0.00011, and the time increment is $\Delta t=(C/U)/2000$ in the present calculations.

Figure 5 shows a typical calculation result, showing the location of the vortices and the cavity in the crossflow plane at each chordwise location. In this figure, small dots show the locations of each vortex element, circle shows the diameter of the cavity, and solid line is the trajectory of the center of cavity. The trajectory of the cavity twists and kinks. This is caused by the velocity by the rolled up vortex. Many vortices in the cavity are caused by the method of the present calculation in which only the effect of the cavity volume change is included in this calculation.

For the flat plate foil, we have lager pressure difference at the leading edge. Hence, the velocity of leakage jet is higher, and the pressure decreases rapidly caused by the strong circulation of the rolled up vortices. Therefore, the cavity initiates and grows rapidly near the leading edge. When the radius of the cavity increases near S/C=0.25, the vortices are washed away caused by the source q_b representing the growth of the cavity. On the contrary, as the radius of cavity decreases near S/C=0.5 caused by the increase of the ambient pressure, the vortices are gathered by the sink representing the effect of the cavity collapse.

Figure 6 shows a typical photograph of the tip leakage vortex cavitation in the experiment. In this photograph, the location and size of the calculated cavity as shown in Fig. 5 is duplicated. Although there are several assumptions in this simple calculation, the qualitative agreement could be found for the location and size of the cavity. In the following section, the trajectory and radius of the cavity in calculations will be compared with experiments under the several conditions.

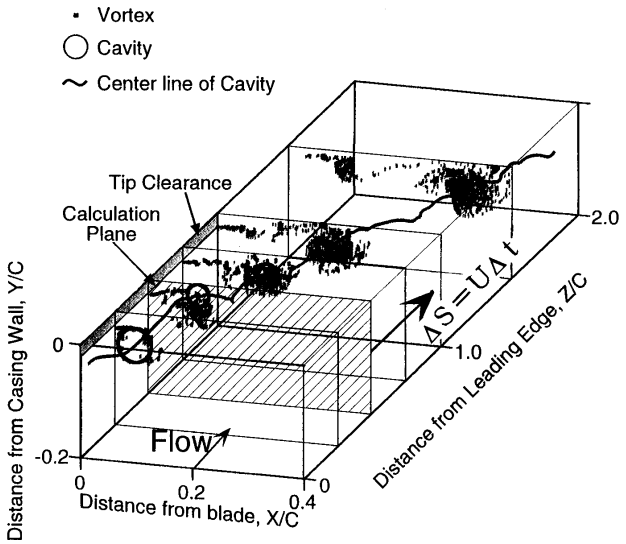

Figure 5 Typical calculation results, for flat plate hydrofoil, α=4 degrees, σ=1.0, and τ=3mm. Vortices and cavity on 2-D crossflow planes arranged in S=U×t

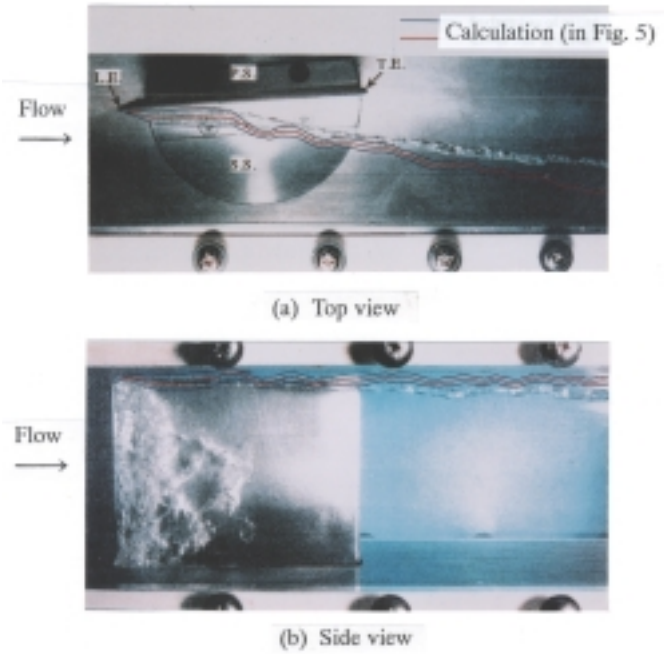

Figure 6 Calculation result (in Fig.5) plotted on the photograph to compare with experiment, for flat plate foil, α=4 degrees, σ=1.0, and τ=3mm

5 Results and discussions

Cavity type. First, we observed the cavity type in the leakage flow for the case of the flat plate foil at several cavitation numbers, angles of attack α=2, 4, 6 degrees, and the tip clearance τ=3 mm. Figure 7 shows the sketch of the tip leakage vortex cavitation and the blade cavitation in four regions shown in Fig. 8 classified from the configurations of the cavity.

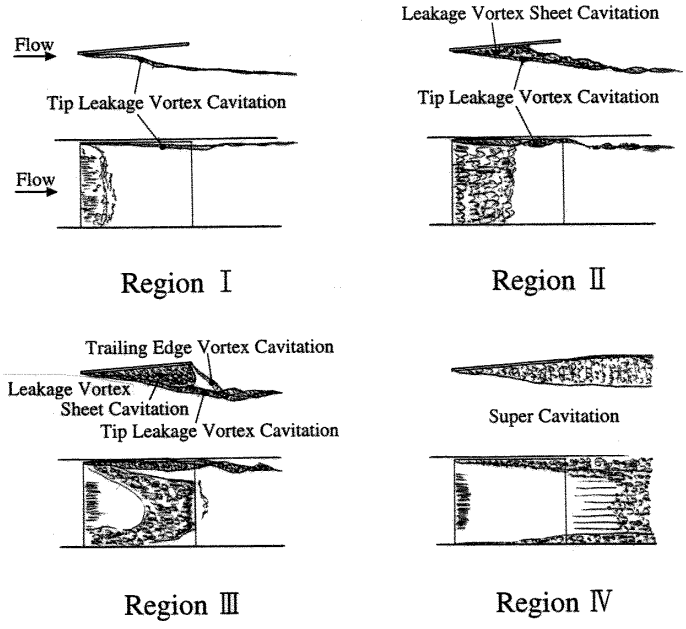

Figure 7 Sketch of tip leakage cavitation and blade cavitation, classified into 4 regions based on the configuration of cavitation

Ⅰ: At higher cavitation number, inception of a string cavitation was observed intermittently near the leading edge at the tip. As the cavitation number decreases, a cylindrical tip leakage vortex cavitation occurs in the leakage vortex. In this region, only this cavitation extends downstream. The end of the cavity is out of the window of the test section.

Ⅱ: At cavitation number lower than Region Ⅰ, the vortex sheet cavitation in the shear layer of leakage flow appeared from the corner of the tip near the leading edge. This leakage vortex sheet cavitation is rolled up into the tip leakage vortex cavitation, and the tip leakage vortex cavitation develops.

Ⅲ: As the cavitation number decreases further, secondary vortex cavitation appears from the tip near the trailing edge. This trailing edge vortex cavitation rotates with the same direction as the tip leakage vortex cavitation. The trailing edge vortex merges with the tip leakage vortex cavitation as it extends downstream. The cavity collapses and disappears after the merger. Similar observation was made by Farrel et al. (1994). They observed the trailing edge vortex cavitation in an axial pump impeller. Through the flow visualization (Zierke et al., 1995), and CFD analysis (Lee et al., 1997), they discussed that the trailing edge vortex cavitation appeared at the core of the separation vortex on the suction side of the blade. Unfortunately, the cause of the trailing edge vortex cavitation could not be made clear from the present experiment.

Ⅳ: As we decrease the cavitation number lower than that in Region Ⅲ, the cavity begins to oscillate. The tip leakage cavitation and the blade cavitation oscillate in phase. If the cavitation number decreases further, the cavity becomes to a super cavity, and the oscillation vanishes. The cylindrical cavitation could not be observed at all in this region.

Figure 8 (a) shows the Region Ⅰ ～Ⅳ on α-σ plane. In addition, Fig. 8 (b) shows the cavity length L on the blade cavitation in comparison with Geurst's analysis (1959). Here, the cavity length L is the mean value at the mid-span. The cavity length of the blade cavitation depends on σ/α theoretically. It is interesting to note here that boundaries of Region Ⅰ ～Ⅳof the leakage cavitations corresponds to the σ/α=constant lines.

In the following section, we focus on the cylindrical vortex cavitation in Region Ⅰ. The conditions, (α, σ), for the calculation are plotted in Fig. 8 (a) with symbols "•".

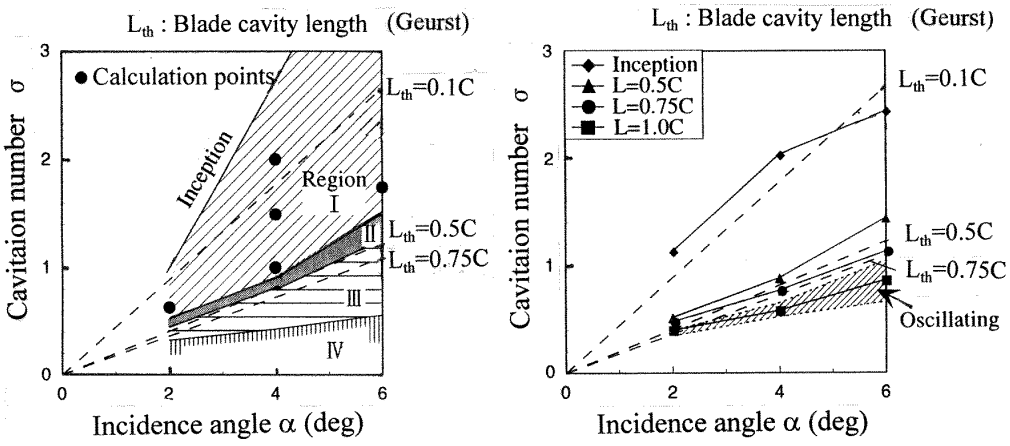

(a) Cavitation maps showing 4 regions in Fig. 7 (b) Cavity length of blade cavitation

Figure 8 Cavitation maps showing 4 regions in Figure 7, and cavity length of blade cavitation compared with Geurst (1959) for flat plate foil

Influence of angle of attack. First, the influence of angle of attack was examined at typical cavitation numbers [(σ, α)=(2 degrees, 0.62), (4 degrees, 1.0), and (6 degrees, 1.75)] for the flat plate foil with the tip clearance τ=3 mm. In these conditions, the cavity length of the blade cavitation was about 40% of the chord length. Figure 9 shows the location and size; i.e., trajectory and radius of the cavity in the experiments. We evaluated the radius of the cavity assuming that the cross section of the tip leakage vortex cavitation is circular. The trajectory of the center of cavity

was measured with the high-speed video pictures from the top and side views. The location and size of the vortex cavitation fluctuate. Error bars in Fig. 9 (b) express the range of the cavity radius fluctuation estimated from the high-speed video pictures. The mean lines show the averaged value at each location. The fluctuation is larger where the cavity is larger. Hereafter we focus only the mean value.

Figure 9 (a) shows the comparison of the trajectory of cavity for the several angles of attack. In this figure, the dotted line ($X=0.46\times(C_L/2)^{1/2}\times Z$, $C_L=2\pi\times\sin\alpha$) shows the empirical one proposed by Chen et al. (1991). This simple relation favorably predicts the influence of the angle of attack on the trajectory of cavity. Figure 10 shows the results of the flow visualizations in case of α=4 degrees. Figure 10 (a) shows the oil-pattern on the upper wall, and Fig. 10 (b) shows the streak of air bubble that was injected at the upper wall on the leading edge. Although those visualizations were made in non-cavitating flow, the trajectory of the cavity as shown in Fig. 6 agrees well with the separation line observed in the oil-pattern, and with the streak of the air bubble. From these results, it could be concluded that the cavitation occurs at the core of the tip leakage vortex, and the influence of the blade cavitation on the trajectory of the tip leakage vortex cavitation is small at least in Region I .

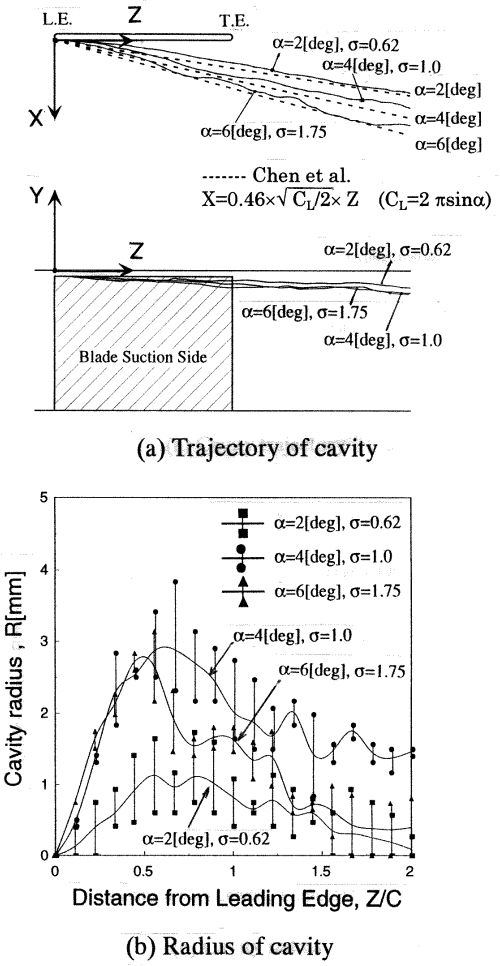

Figure 9 Experimental results of location and size of cavity. (a) Trajectory of cavity and (b) Radius of cavity, for flat plate foil, τ=3mm. Trajectory of cavity is compared with the trajectory of leakage vortex proposed by Chen et al. (1991). Radius of cavity is shown with mean value and the range of fluctuation

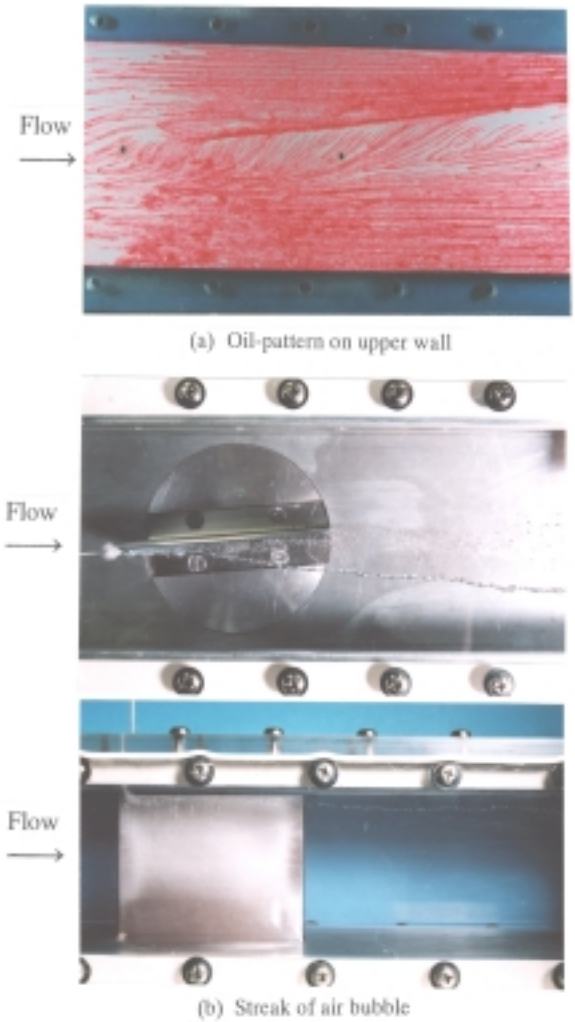

Figure 10 Flow visualization, (a) Oil-pattern on upper wall showing the separation line, and (b) Streak with air bubble, for flat plate foil, α=4 degrees, τ=3mm in non-cavitating flow

Figure 11 shows the comparison of the trajectory and radius of the cavity between the experiments and calculations. Both results show the same behavior with respect to the angle of attack. For the trajectory of the cavity in Fig. 11 (a), the angle made by the foil and the trajectory of the cavity increases as the angle of attack increases. However, the angle of attack has no influence on the location of the cavity in Y-direction. The distances between the trajectory and the upper wall are almost equal to the tip clearance τ. For the radius of the cavity in Fig. 11 (b), the experiment shows that the cavity initiates at the leading edge, and becomes the largest value at Z/C =0.5. After that, the size of cavity decreases gradually. However, the calculation results shows that the cavity grows rapidly near the leading edge, and becomes the largest value at about Z/C=0.3. Then, the cavity size decreases sharply. Although the agreement between the experiment and calculation is not sufficient quantitatively, the same tendency could be found with respect to the influence of the angle of attack.

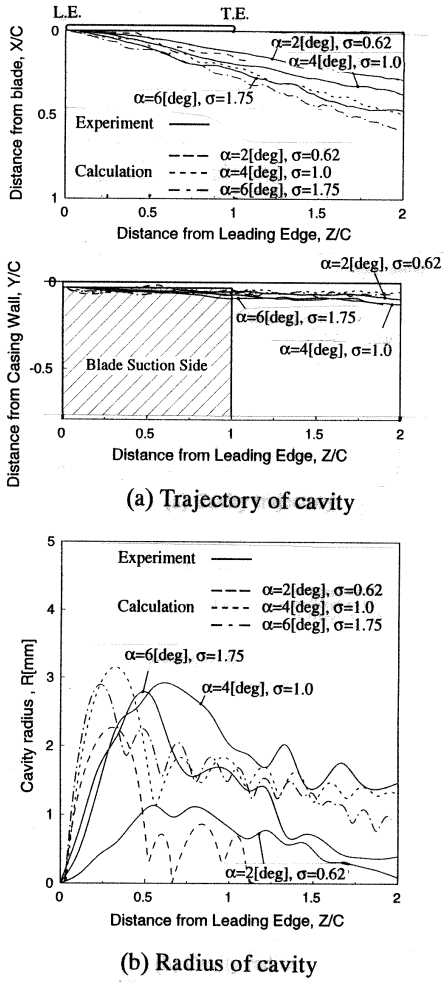

Figure 11 Comparison of the trajectory and radius of cavity between experiment and calculation, showing the effect of the attack angle α=2, 4, 6 degrees, for flat plate foil, and τ=3mm

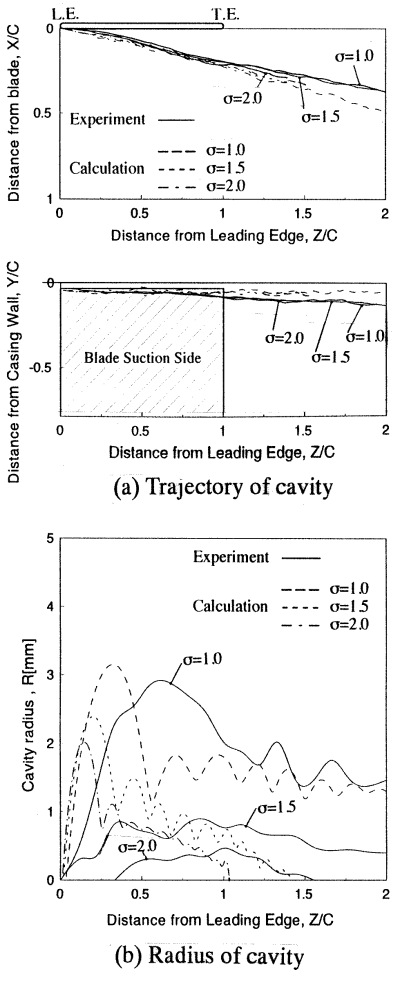

Fig. 12 Comparison of the trajectory and radius of the cavity between experiment and calculation, showing the effect of the cavitation numbers σ=1.0, 1.5, 2.0, for flat plate foil, α=4 degrees, and τ=3mm

Influence of cavitation number. Figure 12 shows the influences of the cavitation number (σ=1.0, 1.5, and 2.0) on the trajectory and radius of the cavity for α=4 degrees, and τ=3 mm. From Fig. 12 (a), it was found that the cavitation number has almost no effect on the trajectory of cavity. However, the initiation and growth of the cavity are affected by the cavitation number as expected. In the experiment, at the higher cavitation number of σ=2.0, the cavitation initiates in the leakage vortex far from the foil at Z/C=0.4, and disappear at the downstream of the foil. At lower cavitation number of σ=1.0, the cavitation appears at the leading edge and develops rapidly. The radius becomes maximum near the Z/C=0.5. On the other hand, the calculation results show that the cavitation number also doesn't affect on the trajectory of the cavity. The radius of cavity increases as the cavitation number decreases. The cavity grows sharply near the leading edge at any cavitation numbers. This tendency is general in the present calculation as shown in Fig. 11. We overestimate the growth of the cavity near the leading edge in the calculation. It seems that the estimation of the pressure difference, Δp, across the tip clearance from the 2-D invisid flow analysis is responsible for the overestimation.

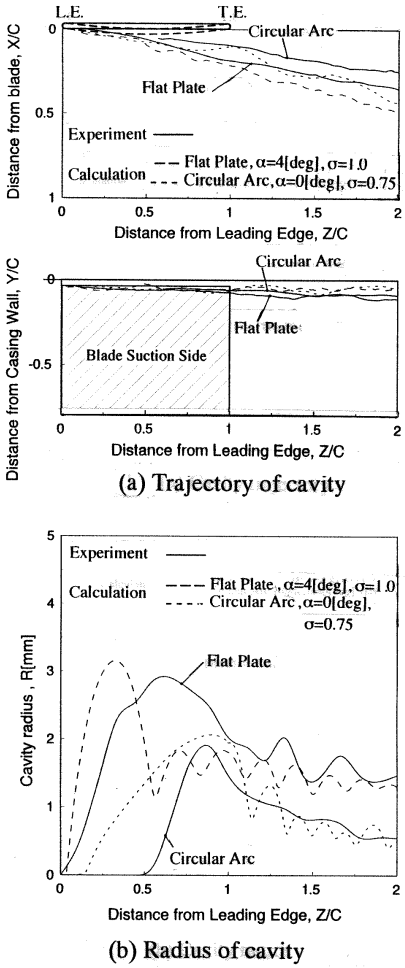

Figure 13 Comparison of the trajectory and radius of the cavity between experiment and calculation, showing the effect of the blade loading distribution, for flat plate foil and circular arc foil, τ=3mm

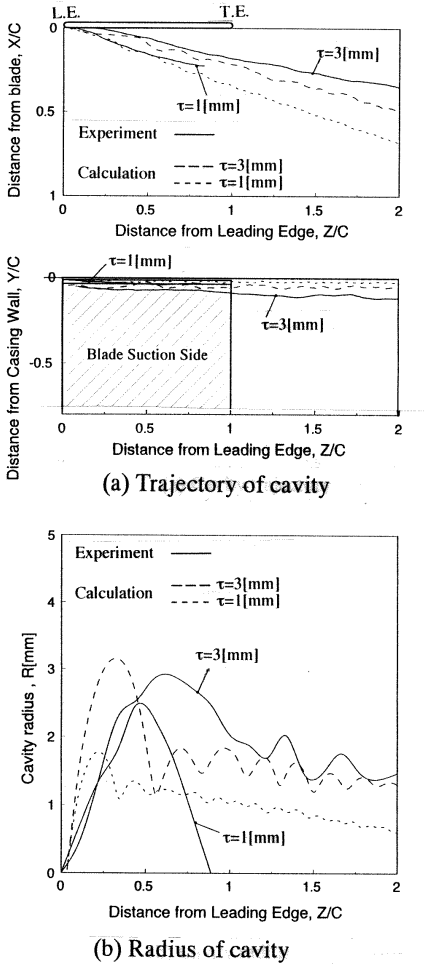

Figure 14 Comparison of the trajectory and radius of the cavity between experiment and calculation, showing the effect of the tip clearance τ=3mm and τ=0.8mm, for flat plate foil, α=4 degrees, and σ=1.0

Influence of blade loading. To examine the influence of the distribution of the blade loading, the experiment was performed by using circular arc foil with the camber $\gamma = 1/2 \cdot \tan\beta$ ($\beta = 4$ degrees.) Although the lift coefficient, C_L, of the circular arc foil for the angle of attack α=0 degree is the same as that of the flat plate foil for α=4 degrees, the distribution of the pressure difference, ΔC_p, is different as shown in Fig. 3. There is no pressure difference at the leading edge in the circular arc foil.

Figure 13 compares the experimental results with the calculation ones. For the circular arc foil, the cavity initiates near Z/C=0.5. The blade cavitation was not observed at this cavitation number σ=0.75. The radius of the cavity increases up to Z/C=0.8, and decreases gradually. Although the cavitation number σ=0.75 for the circular arc foil is lower than that σ=1.0 for the flat plate foil, the radius of cavity for the circular arc foil is smaller than that for the flat plate foil in both experiment and calculation. From these comparisons, it was found that the calculation simulates the effects of the blade loading distribution qualitatively as to the location where the cavity initiates, and the size of cavity.

Influence of tip clearance. The tip clearance was decreased from τ=3.0 mm to τ=0.8 mm for the flat plate foil case. In this case, the ratio of clearance to span is τ/H=0.011. Janigro et al. (1973) examined the experimental results of inducers, and reported that the optimum clearance for the cavitation performance was from 0.008 to 0.01 of the blade height.

Figure 14 shows the trajectory and the radius of cavity compared between τ=3.0 mm and 0.8mm. The radius of cavity for the narrow tip clearance is smaller than that for wider clearance even at the same cavitation number $\sigma = 1.0$. The angle made by the foil and the trajectory of the cavity for the narrow tip clearance is larger than that for the wider clearance. These tendencies could be observed in the calculation results. This can be explained from the distribution of the vortices as follows.

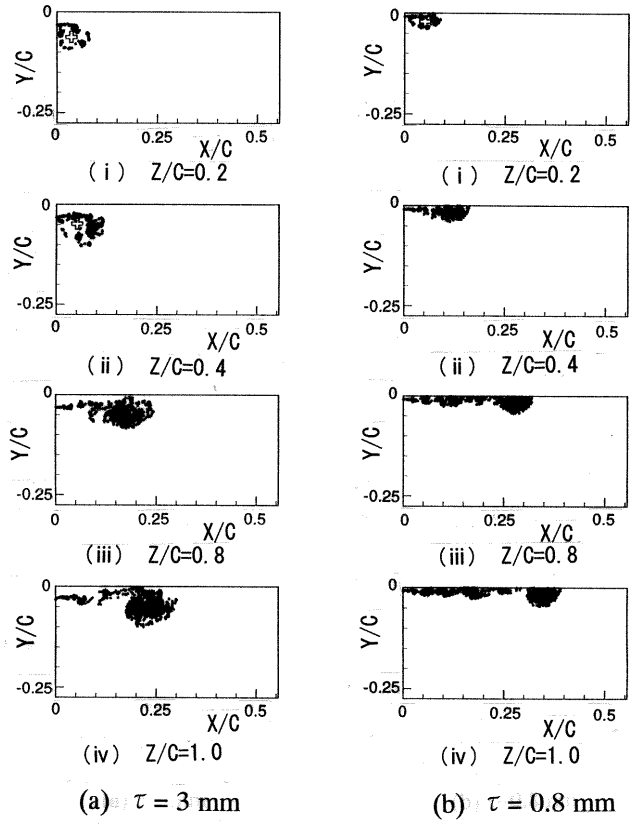

Fig. 15 Comparison of the distributions of vortices in case of (a) τ=3mm, and (b) τ=0.8mm, for flat plate foil, α=4 degrees, and σ=1.0

Figure 15 shows the comparison of the locations of the vortices for τ=3 mm, and τ=0.8 mm in several crossplanes. For the case of the wider clearance, the vortex develops earlier by rolling up of the vortices. This is mainly because there is enough space to form the vortex. The pressure in the vortex core decreases rapidly, and the cavity grows. On the other hand, for the narrow clearance, the free vortices are convected further away along the upper wall. The smaller distance between the vortices and the upper wall hinders the rolling up of the vortices. For this reason, the pressure drop caused by the circulation is smaller than that for the wider clearance, and the growth of the cavity is suppressed.

In this section, we have compared the experimental results with the calculation results in several conditions. Although the simulation uses various simplifying assumptions described in the analytical model, it was found that the simulation can predict qualitatively the influence of the angle of attack, cavitation number, blade loading distributiuon, and the size of the tip clearance on the tip leakage vortex cavitation.

6 Conclusions

Results obtained in the present study can be summarized as follows.

(1) The cavitations in the leakage flow could be classified into the four types. The regions for each type of cavitation were shown in σ-α plane. In case of the flat plate foil, the boundaries of these regions almost coincide with σ/α=constant lines.

(2) The 2-D unsteady flow model based on a slender body approximation can qualitatively predict the location, and the size of the cavity.

(3) The location of the cavity is affected by the angle of attack, but not by the cavitation number. The size of cavity is affected by both the angle of attack and the cavitation number.

(4) The location where the cavity initiates in the tip leakage flow depends on the blade loading. The size of the cavity for a circular arc foil is smaller than that for the flat plate foil under the condition with the same lift coefficient.

(5) The size of the tip leakage vortex cavitation is smaller for the case with narrow tip clearance than the wider tip clearance. From the 2-D calculations, it was found that it is caused by the fact that the roll up of the vortices is hindered for the case with small tip clearance.

Acknowledgement

This study was motivated by a discussion of one of the author (Y. T.) with Prof. Allan Acosta. The authors would like to express their sincerer gratitude for his continued interests and suggestions. They would also like to thank to Dr. Kotaro Sato of Kougakuin University, and Dr. Satoshi Watanabe of Kyusyu University who made many valuable discussions for the experiments and calculations, and Mr. Tetsuji Kuwabara of NAC Inc. for their continued experimental support. This study was partly supported by the Grand-in-Aid for Science Research of the Ministry of Education, Science, Sports, and Culture.

References

Arndt, R. E. A., and Kellen, A. P., 1992, “Water Quality Effects on Cavitation Inception in a Trailing Vortex,” ASME *Journal of Fluids Engineering*, Vol. 114, pp.430-438

Brennen, C. E., 1978, “Bubbly Flow Model for Dynamic Characteristics of Cavitating Pumps, ” *Journal of Fluid Mechanics*, Vol. 89, pp. 234-240

Chen, G. T., Greitzer, E. M., Tan, C. S., and Marble, F. E., 1991, “Similarity Analysis of Compressor Tip Clearance Flow Structure,” ASME *Journal of Turbomachinery*, Vol. 113, pp. 260-271

Farrel, K. J., and Billot, M. L., 1994, “A Correlation of Leakage Vortex Cavitation in Axial-Flow Pumps,” ASME *Journal of Fluids Engineering*, Vol. 116, pp. 551-557

Gearhart, W. S., 1966, “Tip Clearance Cavitation in Shrouded Underwater Propulsors,” AIAA *Journal of Aircraft*, Vol. 3, No.2, pp.1852-192

Geurst, J. A., 1959, “Linearized Theory for Partial Cavitated Hydrofoils,” *Int. Shipbuilding Progress*, Vol. 6, No. 60, pp.369-384

Green, S. I., 1991, “Correlating Single Phase Flow Measurements with Observations of Trailing Vortex Cavitation,” ASME *Journal of Fluids Engineering*, Vol. 113, pp. 125-129

Ido, A., and Uranishi, K., 1991, “Tip Clearance Cavitation and Erosion in Mixed-Flow Pumps,” ASME FED-Vol.119, pp.27-29

Janigro, A., and Ferrini, F., 1973, “Recent Progress in Pump Research,” V.K.I., Lecture Series 61

Laborde, R., Chantrel, P., and Mory, M., 1997, "Tip Clearance and Tip Vortex Cavitation in Axial Flow Pump," ASME *Journal of Fluids Engineering*, Vol.119, pp. 680-685

Lee, Y. T., Laurita, M., Feng, J., and Merkle, C. L., 1997, "Characteristics of Tip-Clearance Flows of A Compressor Cascade and A Propulsion Pump," ASME Paper 97-GT-36

Otsuka, S., Tsujimoto, Y., Kamijo, K., and Furuya, O., 1996, "Frequency Dependence of Mass Flow Gain Factor and Cavitation Compliance of Cavitating Inducers," ASME *Journal of Fluids Engineering*, Vol. 118, pp. 400-408

Rains, D. A., 1954, "Tip Clearance Flows in Axial Flow Compressors and Pumps," *California Institute of Technology, Hydrodynamics and Mechanical Engineering Laboratories*, *Labo. Rep*. No. 5

Watanabe, S., Seki, H., Higashi, S., Yokota, K., and Tsujimoto, Y., 2001, "Modeling of 2-D Leakage Jet Cavitation as a Basic Study of Tip Leakage Vortex Cavitation," ASME *Journal of Fluids Engineering*, in prints

Zierke, W. C., Farrel, K. J., and Strake, W. A., 1995, "Measurements of the Tip Clearance Flow for a High-Reynolds-Number Axial Flow Rotor," ASME *Journal of Turbomachinery*, Vol. 117, pp.522-532